Cell Reports Medicine, Volume *4*

Supplemental information

Pre-existing Fc profiles shape the evolution of neutralizing antibody breadth following influenza vaccination

Carolyn M. Boudreau, John S. Burke IV, Alexander L. Roederer, Matthew J. Gorman, Sophia Mundle, Daniel Lingwood, Simon Delagrave, Saranya Sridhar, Ted M. Ross, Harry Kleanthous, and Galit Alter

Influenza strain	Abbreviation
H1N1 A/South Carolina/1/1918	H1SC18
H1N1 A/Puerto Rico/8/1934	H1PR34
H1N1 A/Weiss/1943	H1We43
H1N1 A/Fort Monmouth/1/1947	H1FM47
H1N1 A/Denver/1957	H1De57
H1N1 A/New Jersey/1976	H1NJ76
H1N1 A/USSR/90/1977	H1USSR77
H1N1 A/Brazil/11/1978	H1Bz78
H1N1 A/California/10/1978	H1CA78
H1N1 A/Chile/1/1983	H1Ch83
H1N1 A/Singapore/6/1986	H1Si68
H1N1 A/Texas/36/1991	H1TX91
H1N1 A/Beijing/262/1995	H1Bei95
H1N1 A/New Caledonia/29/1999	H1NC99
H1N1 A/Solomon Islands/03/2006	H1SI06
H1N1 A/Brisbane/59/2007	H1Br07
H1N1 A/California/07/2009	H1CA09
H1N1 A/Michigan/45/2015	H1Mi15
H3N2 A/Hong Kong/1/1968	H3HK68
H3N2 A/Port Chalmers/12/1973	H3PC73
H3N2 A/Texas/1/1977	H3TX77
H3N2 A/Mississippi/1/1985	H3MS85
H3N2 A/Sichuan/60/1989	H3Sich89
H3N2 A/Shangdong/9/1993	H3Shan93
H3N2 A/Nanchang/933/1995	H3Nan95
H3N2 A/Sydney/5/1997	H3Syd97
H3N2 A/Panama/2007/1999	H3Pa99
H3N2 A/Fujian/411/2002	H3Fu02
H3N2 A/New York/55/2004	H3NY04
H3N2 A/Wisconsin67/2005	H3WI05
H3N2 A/Brisbane/10/2007	H3Br07
H3N2 A/Kentucky/UR07-0028/2008	H3Ur07
H3N2 A/Perth/16/2009	H3Pe09
H3N2 A/Victoria/361/2011	H3Vi11
H3N2 A/Texas/50/2012	H3TX12
H3N2 A/Switzerland/9715293/2013	H3Sw13
H3N2 A/Hong Kong/4801/2014	H3HK14
B/Lee/1940	BLee40
B/Yamagata/16/1988	BYam88
B/Harbin/7/1994	BHar94
B/Sichuan/379/1999	BSich99
B/Hong Kong/330/2001	BHK01
B/Malaysia/2506/2004	BMal04
B/Florida/4/2006	BFL06
B/Brisbane/60/2008	BBr08
B/Wisconsin/1/2010	BWI10
B/Texas/06/2011	BTX11
B/Massachusetts/2/2012	BMA12
B/Phuket/3073/2013	BPh13
B/Colorado/06/2017	BCO17

Table S1.
Influenza strains tested in HAI assays, Related to Figure 1A.

Influenza strain	Abbreviation	Ag-specific Ab isotype titers & FCR binding		Ag-specific Ab isotype & FcR binding affinity		Ag-specific Ab functions		Ag-specific Ab glycosylation	
		Cohort 1	*Cohort 2*	*Cohort 1*	*Cohort 2*	*Cohort 1*	*Cohort 2*	*Cohort 1*	*Cohort 2*
		FCGR2A *FCGR2B* *FCGR3A* *IgA1* *IgG1* *IgG3* *IgM* *Total IgG*	*FCGR2A* *FCGR2B* *FCGR3A* *FCGR3B* *IgA1* *IgA2* *IgG1* *IgG2* *IgG3* *IgG4* *IgM*		*FCGR2A* *FCGR2B* *FCGR3A* *FCGR3B* *IgA1* *IgA2* *IgG1* *IgG2* *IgG3* *IgG4* *IgM*	*ADCP* *ADNP* *ADCD* *ADNKA* *ADDCP*	*ADCP* *ADNP* *ADCD*		
H1N1 A/Chile/1/1983	H1Ch83	HA	HA		HA				
H1N1 A/New Caledonia/29/1999	H1NC99	HA	HA		HA				
H1N1 A/Brisbane/59/2007	H1Br07	HA	HA		HA				
H1N1 A/California/07/2009	H1CA09	HA, NA	HA, NA		HA, NA	HA	HA	HA	
H1N1 A/Michigan/45/2015	H1Mi15		NA		NA				
H1N1 A/Belgium/145-MA/2009	H1Be09		NA		NA				
H1 stabilized stem	H1 stem	HA	HA		HA				
H3N2 A/Panama/2007/1999	H3Pa99	HA	HA		HA				
H3N2 A/Brisbane/10/2007	H3Br07	HA	HA		HA				
H3N2 A/Texas/50/2012	H3TX12	HA, NA	HA, NA		HA, NA	HA	HA	HA, NA	
H3N2 A/Switzerland/9715293/2013	H3Sw13	HA	HA, NA		HA, NA				
H3N2 A/Hong Kong/4801/2014	H3HK14	HA, NA	HA, NA		HA, NA				
H3N2 A/Singapore/19/2016	H3Si16	HA	HA		HA				
H3 stabilized stem	H3 stem		HA		HA				
B/Brisbane/60/2008	BBr08	HA	HA		HA				
B/Phuket/3073/2013	BPh13	HA	HA, NA		HA, NA				
B/Colorado/06/2017	BCO17	HA	HA, NA		HA, NA				

Table S2.

Systems serologic measurements by sample cohort and influenza strain, Related to Figures 1-4.

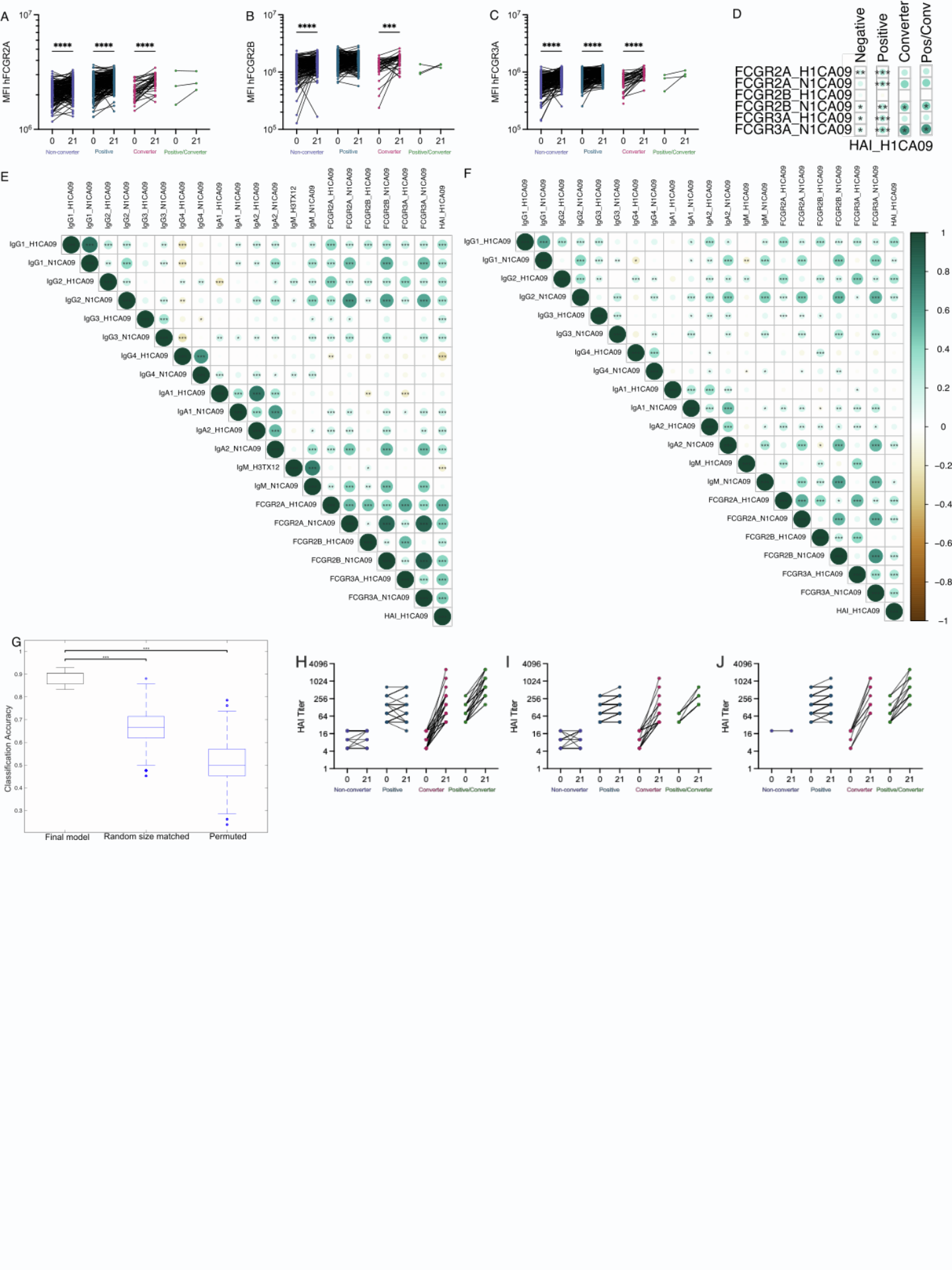
A
MFI hFCGR2A
B
MFI hFCGR2B
C
MFI hFCGR3A
Non-converter
Positive
Converter
Positive/Converter
D
Negative
Positive
Converter
Pos/Conv
FCGR2A_H1CA09
FCGR2A_N1CA09
FCGR2B_H1CA09
FCGR2B_N1CA09
FCGR3A_H1CA09
FCGR3A_N1CA09
HAI_H1CA09
E
F
G
Classification Accuracy
Final model
Random size matched
Permuted
H
I
J
HAI Titer

Figure S1. *HAI titers, influenza-specific antibody isotype levels, and influenza-specific FcgR binding levels are highly correlated pre-vaccination but come partially unlinked in the response to vaccination, Related to Figure 1.* Line plots (A-C) shows before-and-after FcR binding levels against H1N1 A/California/07/2009, with individuals broken out into groups based on HAI seroconversion as described. Significance tested by one-way ANOVA with Holm-Sidak posttest to compare between day 0 versus day 21. **** $p < 0.0001$. Spearman correlations were calculated between antibody measures for delta pre-to-post vaccination samples between HAI and FcR binding by HAI seroconversion groups (D). Spearman correlations were also calculated across the entire population at day 21 post vaccination (E) or delta pre-to-post-vaccination samples (F) in cohort two and plotted using the corrplot package in R. Stronger correlations are represented by larger circles. Asterisks represent significance as calculated by the ggcorplot package for Spearman correlations; * $p < 0.05$, ** $p < 0.01$, *** $p < 0.001$. Box plot (G) shows model accuracy for LASSO classification model, random size matched models, and permuted label models. LASSO was run for 20 replicates of 5-fold data separation. Random size matched and permuted label models were run 100 permutations per replicate. Stars indicate significance by unpaired, two-tailed T tests. *** $p < 0.001$. Line plots show before-and-after HAI titers against (H) H3N2 A/Texas/50/2012, (I) B/Brisbane/60/2008, and (J) B/Massachusetts/2/2012 with individuals broken out into groups based on HAI conversion for each strain: 1) individuals that did not experience seroconversion (non-converters), 2) individuals who were HAI positive prior to vaccination and did not experience significant increase in HAI titer (positives), 3) individuals who had sub-protective HAI titers prior to vaccination but seroconverted following vaccination (converters), and 4) individuals who were HAI positive prior to vaccination but saw a significant (greater than or equal to four-fold) increase in HAI titer following vaccination (positive/converters). This figure represents data from the Investigation cohort.

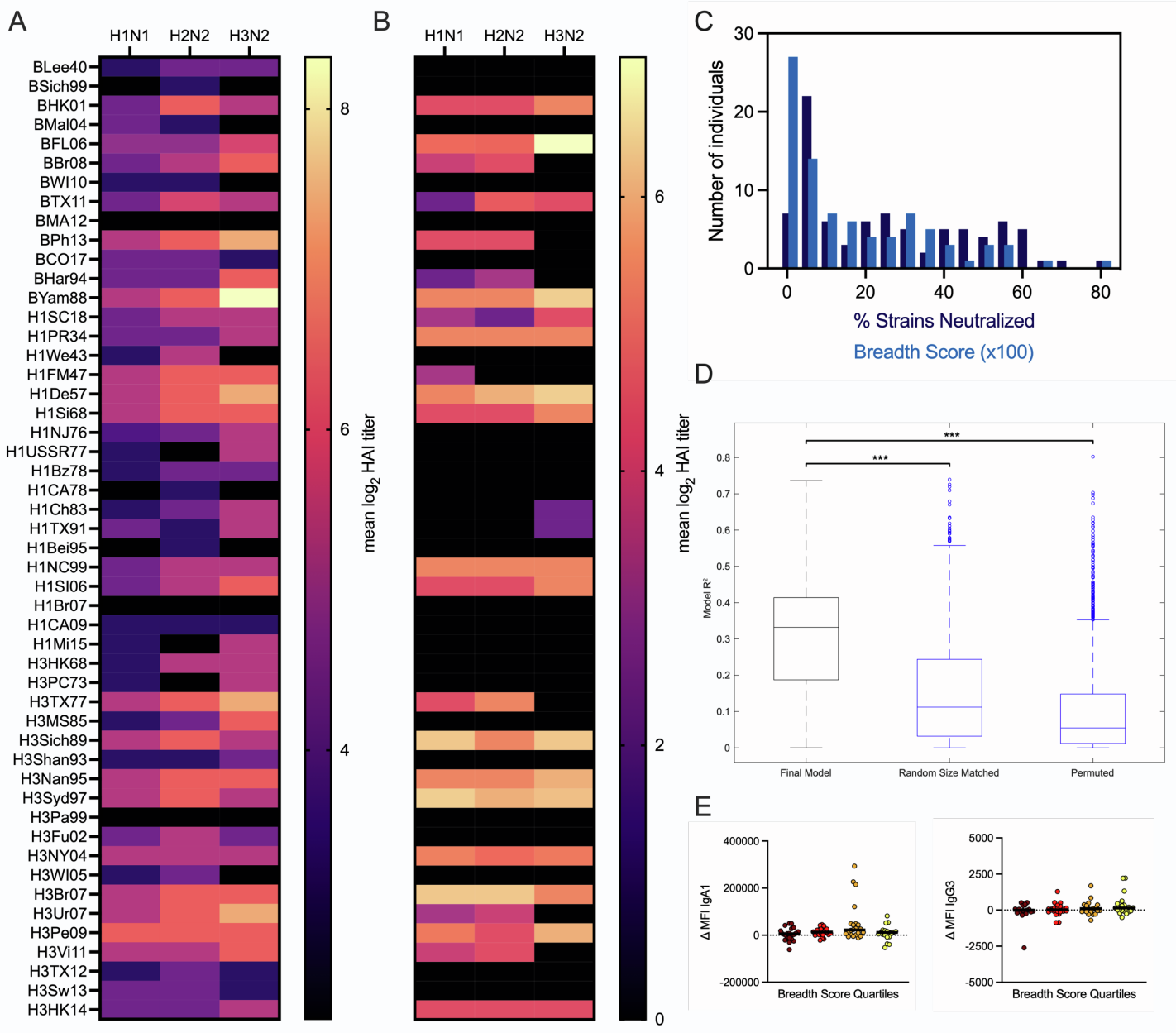

Figure S2.

Pre-existing and vaccine-induced HAI responses are not heavily impacted by immunological imprinting but do correlate with development of FcR binding antibodies, Related to Figure 2.

Individuals from the Investigation cohort were grouped by their year of birth into three discreet immunological imprinting eras (H1N1 1920-1954, H3N2 1955-1966, H3N2 1966-2005 (Arevalo et al., 2020)) with each era represented in a column. Heatmap (A) shows pre-existing responses to each tested virus by row with coloring by the mean log_2-transformed HAI titer for the group; Heatmap (B) shows delta day 21- day 0 vaccine-induced responses. Histogram (C) shows both percentage seroconversion (dark blue) and breadth score (light blue) for the first Discovery cohort. Percentage of strains neutralized does not take into account genetic sequence diversity of strains, while the breadth score does. Box plot (D) shows model accuracy (R^2) for LASSO-Elastic Net classification model in Figure 2, random size matched models, and permuted label models. LASSO-Elastic Net was run for 20 replicates of 5-fold data separation. Random size matched and permuted label models were run 100 permutations per replicate. Stars indicate significance by unpaired, two-tailed T tests. *** $p < 0.001$. Dot plots (E) show additionalLASSO-Elastic Net selected features as univariate plots binned by quartile of breadth score. Significance was tested by Kruskal-Wallis test followed by Dunn's multiple comparisons correction. Not significant.

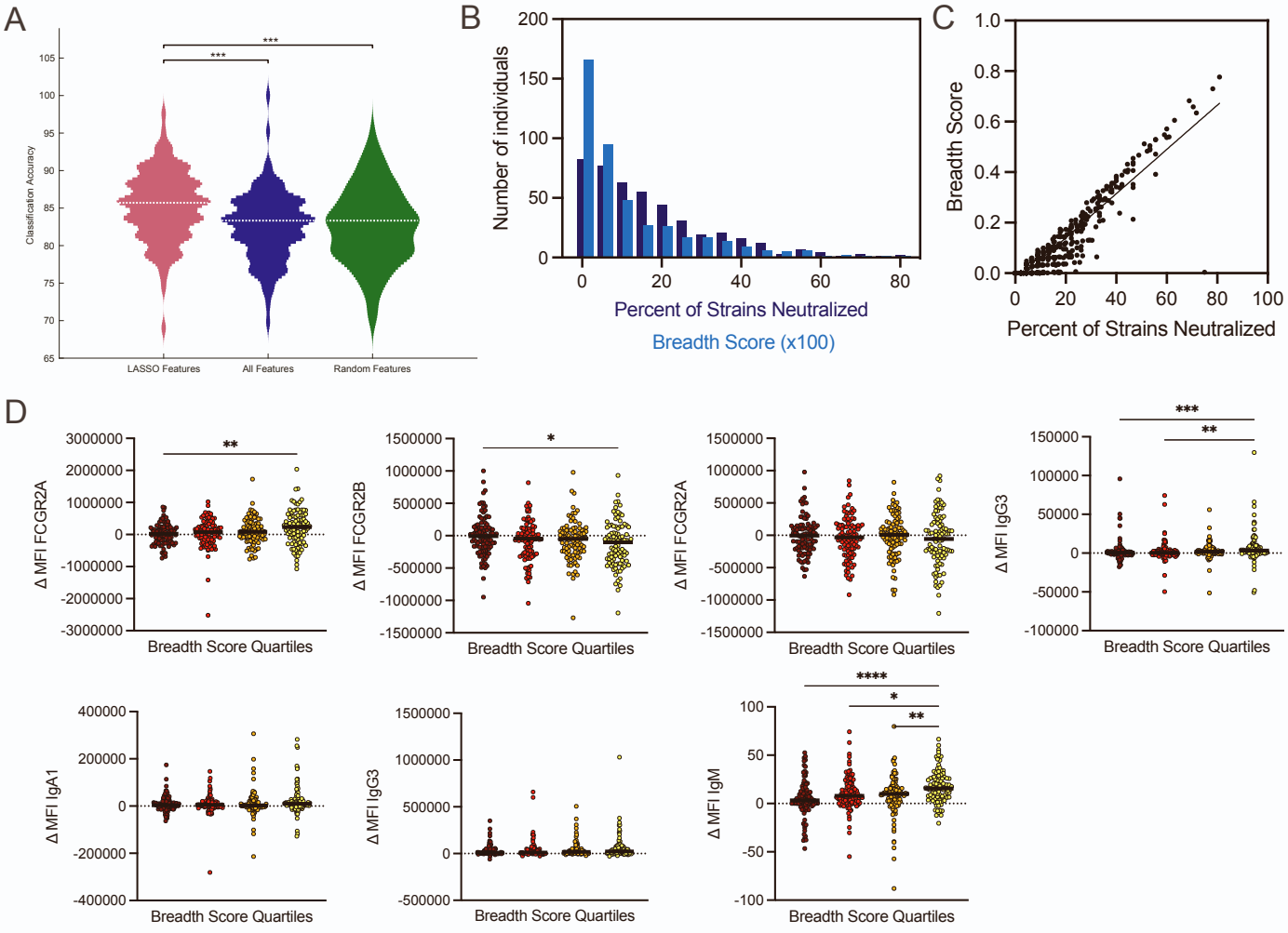

Figure S3.

Validation of the seroconversion model in Figure 1 with an orthogonal cohort, Related to Figure 3.

Violin plot (A) shows comparison of seroconversion model in Figure 1 with an orthogonal cohort. Histogram (B) shows both percentage seroconversion and breadth score for the second Investigative cohort. Dot plot (C) shows correlation between percentage of strains seroconverted and breadth score for the second Investigative cohort. Dot plots (D) show LASSO-Elastic Net selected features as univariate plots binned by quartile of breadth score. Significance was tested by Kruskal-Wallis test followed by Dunn's multiple comparisons correction. * $p < 0.05$, ** $p < 0.01$, *** $p < 0.001$.

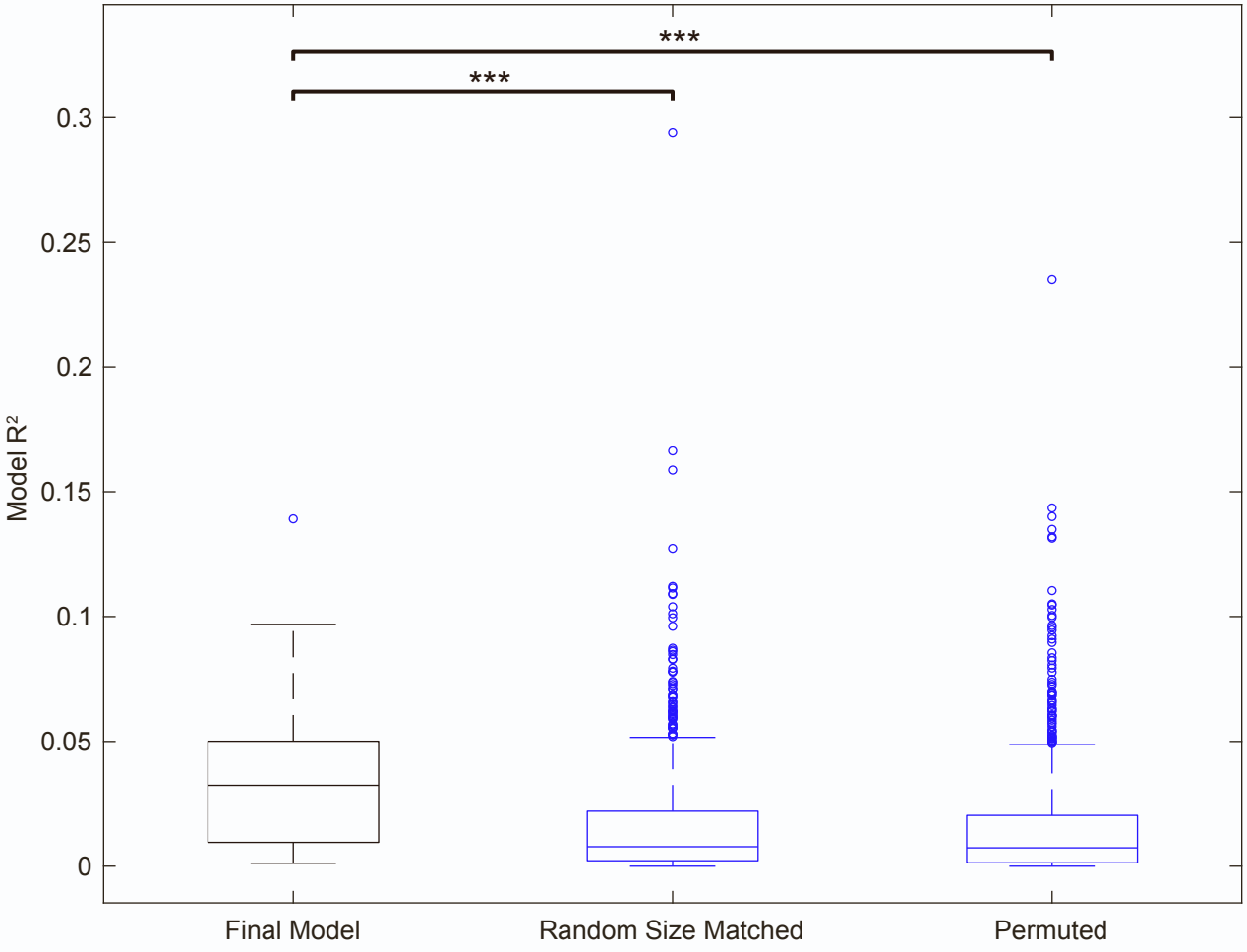

Figure S4.
Accuracy and significance of breadth model in Figure 4A. Box plot shows model accuracy (R^2) for LASSO-Elastic Net classification model, random size matched models, and permuted label models. LASSO-Elastic Net was run for 20 replicates of 5-fold data separation. Random size matched and permuted label models were run 100 permutations per replicate. Stars indicate significance by unpaired, two-tailed T tests. *** $p < 0.001$.

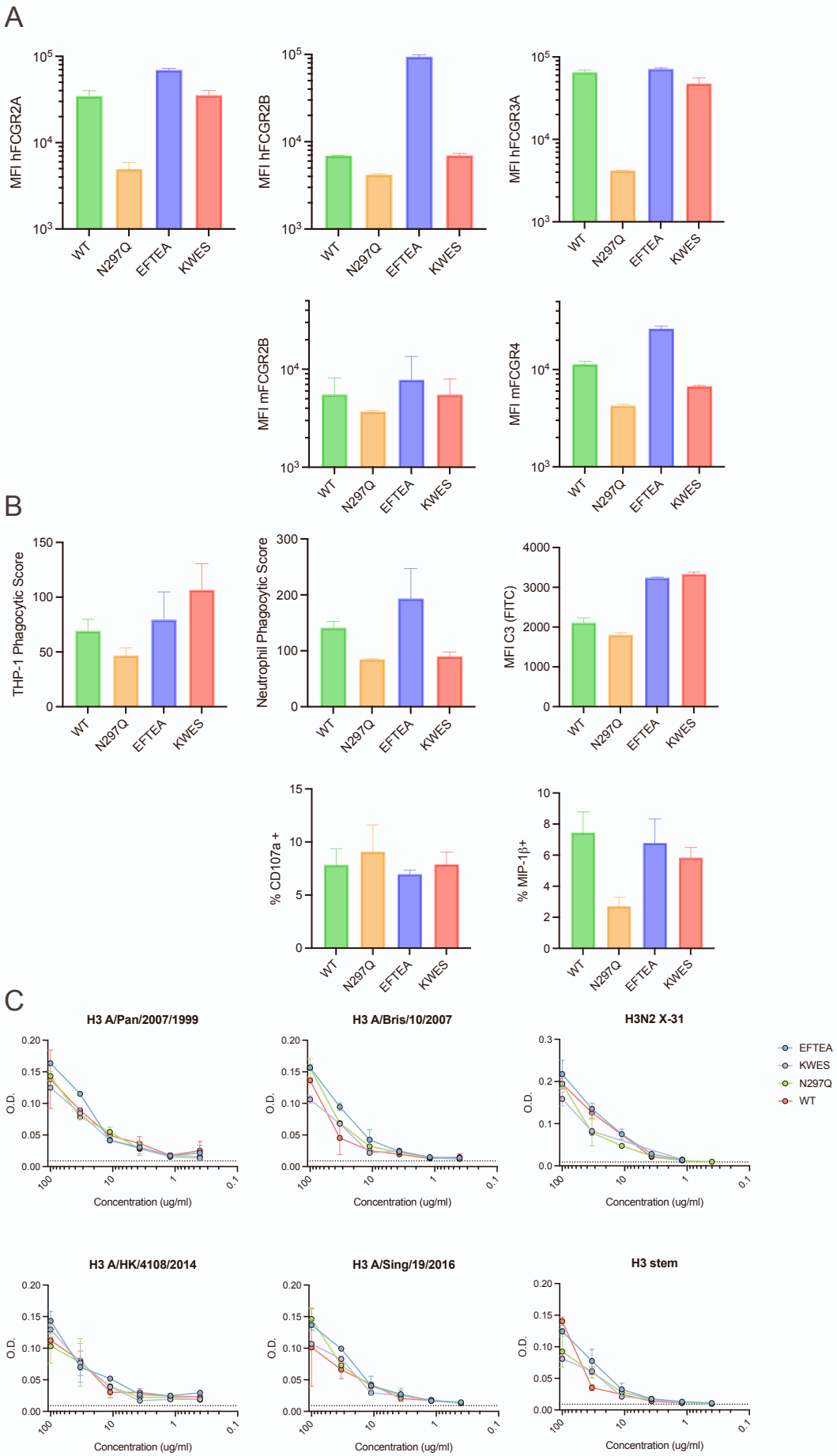
A
MFI hFCGR2A
MFI hFCGR2B
MFI hFCGR3A
MFI mFCGR2B
MFI mFCGR4
WT
N297Q
EFTEA
KWES
B
THP-1 Phagocytic Score
Neutrophil Phagocytic Score
MFI C3 (FITC)
% CD107a +
% MIP-1β+
C
H3 A/Pan/2007/1999
H3 A/Bris/10/2007
H3N2 X-31
H3 A/HK/4108/2014
H3 A/Sing/19/2016
H3 stem
O.D.
Concentration (ug/ml)
EFTEA
KWES
N297Q
WT

Figure S5.
CR9114 Fc variant antibodies show different FcR binding and Fc functional profiles but bind to the same influenza antigens, related to Figure 5. (A) shows relative binding to human and mouse FcgRs by H3 stem-specific Luminex analysis. (B) shows antibody functionality in phagocytosis, complement deposition and NK cell activation. Bars show mean and standard deviation of duplicates. (C) Line plots show serial dilution curves for CR9114 variants binding to H3N2 antigens. Each point represents two independent measurements.

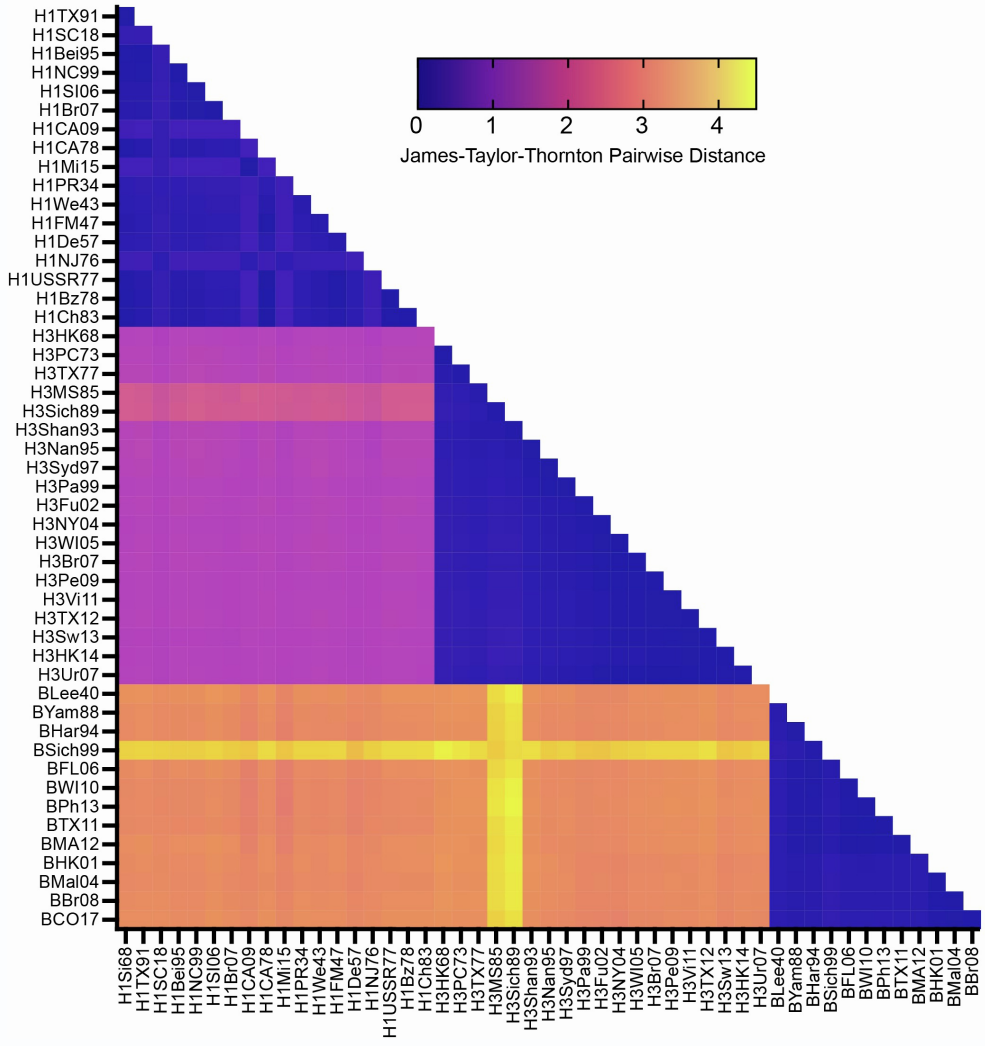

Figure S6.
Pairwise distance between tested strains of influenza, Related to STAR Methods. Heatmap shows James-Taylor-Thornton pairwise distances between each pair of tested influenza strains.